Published in final edited form as:

J Comp Neurol. 2016 April 15; 524(6): 1270–1291. doi:10.1002/cne.23904.

Pontine Reticulospinal Projections in the Neonatal Mouse: Internal Organization and Axon Trajectories

Magne S. Sivertsen[1], **Marie-Claude Perreault**[2], and **Joel C. Glover**[1,3,*]

[1]Laboratory of Neural Development and Optical Recording (NDEVOR), Department of Physiology, Institute of Basic Medical Sciences, Faculty of Medicine, University of Oslo, 0316 Oslo, Norway

[2]Department of Physiology, Emory University School of Medicine, Atlanta, Georgia 30307

[3]Norwegian Center for Stem Cell Research, Oslo University Hospital, 0317 Oslo, Norway

Abstract

We recently characterized physiologically a pontine reticulospinal (pRS) projection in the neonatal mouse that mediates synaptic effects on spinal motoneurons via parallel uncrossed and crossed pathways (Sivertsen et al. [2014] *J Neurophysiol* 112:1628–1643). Here we characterize the origins, anatomical organization, and supraspinal axon trajectories of these pathways via retrograde tracing from the high cervical spinal cord. The two pathways derive from segregated populations of ipsilaterally and contralaterally projecting pRS neurons with characteristic locations within the pontine reticular formation (PRF). We obtained estimates of relative neuron numbers by counting from sections, digitally generated neuron position maps, and 3D reconstructions. Ipsilateral pRS neurons outnumber contralateral pRS neurons by threefold and are distributed about equally in rostral and caudal regions of the PRF, whereas contralateral pRS neurons are concentrated in the rostral PRF. Ipsilateral pRS neuron somata are on average larger than contralateral. No pRS neurons are positive in transgenic mice that report the expression of GAD, suggesting that they are predominantly excitatory. Putative GABAergic interneurons are interspersed among the pRS neurons, however. Ipsilateral and contralateral pRS axons have distinctly different trajectories within the brainstem. Their initial spinal funicular trajectories also differ, with ipsilateral and contralateral pRS axons more highly concentrated medially and laterally, respectively. The larger size and greater number of ipsilateral vs. contralateral pRS neurons is compatible with our previous finding that the uncrossed projection transmits more reliably to spinal motoneurons. The information about supraspinal and initial spinal pRS axon trajectories should facilitate future physiological assessment of synaptic connections between pRS neurons and spinal neurons.

Correspondence: Joel C. Glover, Laboratory of Neural Development and Optical Recording (NDEVOR), Department of Physiology, Institute of Basic Medical Sciences, University of Oslo, PB 1103 Blindern, 0316 Oslo, Norway. joel.glover@medisin.uio.no.

CONFLICT OF INTEREST STATEMENT

The authors have no conflicts of interest associated with this work.

ROLE OF AUTHORS

All authors had full access to all the data in the study and take responsibility for the integrity of the data and the accuracy of the data analysis. Study concept and design: MSS, M-CP, JCG. Acquisition of data: MSS, JCG. Analysis and interpretation of data: MSS, M-CP, JCG. Drafting of the manuscript: MSS, JCG. Critical revision of the manuscript for important intellectual content: MSS, M-CP, JCG. Approval of final manuscript draft: MSS, M-CP, JCG. Statistical analysis: MSS, JCG. Obtained funding: M-CP, JCG. Administrative, technical, and material support: JCG. Study supervision: JCG.

Keywords

descending pathways; brainstem; spinal cord; motor control; bulbospinal; startle reflex; posture; locomotion; AB_1502299; AB_10143907; AB_141784

Most descending projections to the spinal cord in mammals arise from the brainstem (24 of 27 neuron groups of origin [Nudo and Masterton, 1988]; over 70% of projecting neurons [Liang et al., 2011]). Although descending projections from the brainstem are heavily involved in the control of sensory, autonomic, and motor functions, how this control is achieved is poorly understood. One important gap in our knowledge involves the internal organization of brainstem descending projection neuron groups into subpopulations according to different functional phenotypes and axon trajectories within the brainstem and spinal cord.

The neonatal mouse brainstem and spinal cord have become an attractive preparation for studying motor circuitry. Ex vivo preparations of the neonatal mouse spinal cord are capable of generating fictive locomotor activity and this has facilitated both anatomical and physiological studies of the underlying synaptic connections (Kiehn, 2006). With the brainstem attached, it is possible to investigate the descending control of spinal motor circuits with great precision (Szokol et al., 2011; Sivertsen et al., 2014; Kasumacic et al., 2015). Because the structures are small and myelination is still nascent, high-throughput optical methods for physiological investigation are especially feasible (Szokol and Perreault, 2009). Transgenic approaches allow a spectrum of celltype-specific manipulations for probing connectivity and function. Providing more comprehensive information about the organization of descending projections from the brainstem to the spinal cord in the neonatal mouse is therefore valuable to the growing community of investigators using this preparation.

Brainstem projections to the spinal cord begin to develop prenatally, and many have established contact with potential target neurons in the spinal cord by birth (Perreault and Glover, 2013). Several lines of evidence suggest that during development the brainstem sources of these projections are internally patterned by regionally differentiated gene expression and that this patterning gives rise to heterogeneity in axon projections and synaptic targeting (Diaz et al., 1998; Auclair et al., 1999; Glover, 2000; Cepeda-Nieto et al., 2005; Pasqualetti et al., 2007; Perreault and Glover, 2013). Thus, characterization of these projections in neonates is likely to reveal basic features of internal organization that relate to functional connectivity not only during early life but also in the adult.

We recently characterized in the neonatal mouse the pattern of functional connections between pontine reticulospinal (pRS) neurons and spinal motoneurons (MNs), using optical recording of synaptically mediated calcium responses (Sivertsen et al., 2014). We showed that these connections are already established at birth and are mediated by two parallel channels, one involving pRS axons that descend ipsilaterally (uncrossed projection) and the other involving pRS axons that descend contralaterally (crossed projection). Although the ipsilateral projection transmits more faithfully and may be more direct, both pRS projections

elicit responses in axial and limb MNs in cervical, thoracic, and lumbar levels, suggesting that both are involved in coordinating widespread patterns of muscle activation.

This organization into different parallel channels has prompted us to make a more precise analysis of the internal organization of these pRS neuron populations in the neonatal mouse, with a particular focus on comparing the anatomical locations of the ipsilaterally and contralaterally projecting pRS neurons (hereafter referred to as “ipsilateral” and “contralateral” pRS neurons) and their supraspinal axon trajectories and initial spinal funicular destinations. We find that ipsilateral pRS neurons are approximately three times more numerous than contralateral and that the two populations are differentially distributed within the PRF. Ipsilateral pRS neurons are equally divided between rostral and caudal regions corresponding to the oral and caudal pontine reticular nuclei (PnO and PnC), whereas contralateral pRS neurons are more concentrated within the PnO. The two populations are also spatially segregated within the transverse plane, with the contralateral pRS neuron population occupying a domain just ventrolateral to the ipsilateral. The two populations of pRS axons project along distinct trajectories within the brainstem, and as they enter the spinal cord they have an oppositely graded mediolateral distribution within the white matter. Ipsilateral pRS axons are more concentrated medially, within the ventral funiculus (VF), whereas contralateral pRS axons are more concentrated laterally, within the lateral funiculus (LF). Part of this work has been published previously in abstract form (Sivertsen et al., 2013).

MATERIALS AND METHODS

Animals

Experiments were performed with preparations of the brainstem and cervical spinal cord from wild-type mice of the Hsd:ICR (CD-1) strain (Harlan France; n = 27, all P0 except for one P2 mouse that was used for neurofilament immunohistochemistry) or the transgenic strains GAD-67 (Tamamaki et al., 2003; n = 5, P1) and GIN (“GFP-expressing inhibitory neurons”; Oliva et al., 2000; Jackson strain FVB-Tg(GadGFP)45704Swn/J; n = 5, P0). After deep inhalation anesthesia with isoflurane and a craniotomy, pups were decerebrated by transecting the brain between the superior colliculus and the forebrain and then submerged in ice-cold (4 °C), oxygenated (95% O_2 and 5% CO_2), low-calcium, “dissection” artificial cerebrospinal fluid (d-ACSF, containing in mM: glycerol 250, KCl 2, d-glucose 11, $CaCl_2$ 0.15, $MgSO_4$ 2, NaH_2PO_4 1.2, HEPES 5, and $NaHCO_3$ 25). Animals were then eviscerated and the brainstem together with cervical and upper thoracic spinal cord was carefully dissected out. To maximize oxygenation, the cerebellum was removed, and the d-ACSF was exchanged every 5 minutes during the dissection.

All efforts were made to minimize the number of animals used and their suffering in accordance with the European Communities Council directive 86/609/EEC and the National Institutes of Health guidelines for the care and use of animals. All procedures were approved by the Norwegian National Animal Research Authority.

Retrograde labeling of pRS neurons

After transfer of the preparations to room-temperature, oxygenated artificial cerebrospinal fluid (ACSF, containing in mM: NaCl 128, KCl 3, d-glucose 11 $CaCl_2$ 2.5, $MgSO_4$ 1, NaH_2PO_4 1.2, HEPES 5, and $NaHCO_3$ 25), the spinal white matter at the level of the second cervical (C2) ventral root was cut unilaterally. The cut spanned the entire extent of the ventral and lateral funiculi (VF 1 LF) or more restricted regions thereof (defined below). To ensure that the LF was included in its entirety, the cut extended beyond the dorsal limit of the LF into the dorsolateral fasciculus (df). Premade crystals of 3-kDa tetramethylrhodamine-conjugated dextran amines (RDA; Invitrogen, Carlsbad, CA; catalog No. D-3308), alone or in combination (ratio 1:1) with biotin-conjugated dextran amine (BDA; Invitrogen; catalog No. D-7135) were inserted into the cut (Glover, 1995). Four to ten crystals inserted over a period of approximately 3 minutes ensured continuous exposure of the cut axons to high tracer concentration. Preparations were then incubated in the dark for approximately 12 hours to allow retrograde transport of the tracers to both ipsilaterally and contralaterally projecting pRS neurons.

To eliminate the possibility of contamination by unintentional labeling of contralateral axons, in all but one preparation the contralateral spinal cord between C1 and T1 was carefully removed prior to application of RDA/BDA. All application sites and lesions were assessed histologically at the end of the experiment (see below).

Retrograde labeling of restricted subpopulations of pRS axons

To characterize the initial spinal funicular trajectories of pRS axons, in 13 preparations we restricted RDA/BDA application to one of three zones of the VF 1 LF white matter by making smaller cuts of defined circumferential extent. The three zones, denoted zones 1, 2, and 3 from medial to lateral, were of roughly equal size. Zone 1 extended from the midline to the ventral apex of the hemicord and thus encompassed the medial part of the VF. Zone 2 extended from the ventral apex of the hemicord to the longitudinal line along which ventral roots exited the spinal cord (“ventral root line”) and thus encompassed the lateral part of the VF and possibly a small part of the LF. Zone 3 extended from the ventral root line to just beyond the dorsal margin of the LF. In all cases, cuts for tracer application involved the entire thickness of the white matter. All application sites were assessed histologically at the end of the experiment (see below).

Histology and immunohistochemistry

Detailed information about the antibodies used for immunohistochemical procedures is shown in Table 1. After each labeling experiment, the preparations were fixed with 4% paraformaldehyde in phosphate-buffered saline (PBS) for 4 hours, cryoprotected in 20% sucrose in PBS (4–24 hours), and separated into brainstem and spinal cord portions. These were separately embedded in OCT (Tissue-Tek, Sakura, Japan), frozen, and cryostat sectioned either in a single series of 50-μm-thick sections in the parasagittal or transverse plane (brainstem portion) or transverse plane (spinal cord portion) or in an alternating series of 14-μm-thick sections in the transverse plane (for 3D reconstruction of the brainstem portion; see below). Before further analysis, all spinal cord application sites and lesions were examined histologically for completeness. Their extents were evaluated through comparison

with a standard cervical cord section, and preparations that differed from the intended extent by more than 20% in either direction were discarded. Immunohistochemistry for neurofilaments (Table 1) was performed on 12-μm transverse sections from a spinal cord not subjected to retrograde labeling.

The transverse 50-μm sections through the spinal cord and one of the two alternating series of 14-μm transverse sections through the brainstem were stained with methylene blue (Difco Laboratories, West Molesey, Surrey, United Kingdom; 10–20 seconds in 0.3% w/v solution). The second alternating series of 14-μm transverse sections through nine brainstems (n = 3 for VF 1 LF, n = 2 for each of zones 1–3) as well as some series of 50-μm sections were subjected to fluorescent signal enhancement. The combined RDA/BDA labeling was enhanced using either an antirhodamine antibody (Table 1) and a red fluorophore-conjugated secondary antibody (Alexa 555 goat anti-rabbit IgG; Invitrogen; Table 1) or a red fluorophore-conjugated streptavidin (Cy3-streptavidin; Jackson Immunoresearch, West Grove, PA; catalog No. 016-220-084). The signal enhancement achieved by the two methods was comparable, and in both cases much improved compared with the nonenhanced signal. The enhancement made detection of labeled somata more reliable and greatly improved the visualization of labeled neurites (both axons and dendrites).

All sections were coverslipped in gelatin-glycerol (50% v/v glycerol and 20% w/v gelatin in PBS) and photographed with a ProgRes C14 215 camera (Jenoptik) mounted on an AX70 microscope (Olympus) using × 4 (UplanApo, NA 0.16) or × 10 (UplanApo, NA 0.40) objectives. Selected sections were also imaged with a laser scanning confocal microscope (Z-stacks obtained using a Zeiss LSM Pascal 5 confocal microscope at × 20 magnification, Plan Apochromat, NA 0.75).

Spatial distribution maps, soma sizes, and neuron density

To estimate pRS neuron soma size and relate it to position within the PRF, we used two of the VF 1 LF labeled brainstems sectioned at 50 μm in the parasagittal plane to construct spatial distribution maps. Confocal projection images were opened in ImageJ (U.S. National Institutes of Health, Bethesda, MD; http://rsb.info.nih.gov/ij/), and a plug-in was used to trace the outline of labeled neurons. The outlines were submitted to a program written in Python (http://www.python.org) for computation of the neuron area (ParticleDensityDouble; Max Larsson, 2014). The source code of the ImageJ plug-in and the Python program are available online (http://www.hu.liu.se/forskning/larsson-max/software?l=en; NIH, open access). In a drawing program (CorelDraw4x, v14.0), a 2D matrix of 10-μm squares was superimposed onto ×4 images of the sections and aligned using specific landmarks, so that each soma could be assigned rostrocaudal and dorsoventral coordinates. Section number was used to define the mediolateral coordinate. To calculate neuron densities, we applied a grid of 100-μm-sided cubes onto the Excel coordinate database, counting the number of labeled neurons within each cube.

3D reconstructions

Nine brainstems (n = 3 for VF 1 LF; n = 2 for each of zones 1–3) were sectioned at 14 μm in alternating series, of which one was labeled with methylene blue and the other subjected to

fluorescent signal enhancement as described above. Every sixth section in these two series was photographed with a Zeiss Axioskop2 microscope equipped with a motorized stage (Märzhäuser), a CX9000 camera (MBF), and a µ 10 objective (Achroplan, NA 0.25). Images were imported into Neurolucida software (version 8; MBF), and specific section features (section outline and midline in all sections, outlines of distinguishable nuclei based on Paxinos et al. [2007] in one section series, and RDA/BDA-labeled neuronal somata in the other section series) were digitally traced or marked. Marked neurons were also given a digital name tag based on comparison with the structures mapped in the immediately adjacent methylene blue-labeled section, falling into one of the pRS neuron populations defined in Results. The alternating digital section series were then intercalated, allowing the construction of digital 3D models. In the 3D models, the anteroposterior extent of the pRS neuron population spanned approximately 12 or 13 digitized transverse sections. Because the angle we used for the transverse sections was not identical to that used by Paxinos et al. (2007), in part because our material was sectioned after dissection and ex vivo incubation, which permits a more accurate alignment of the rostrocaudal axis, for presentation purposes we added outlines of cytoarchitectonically defined structures and nuclei (including many that were not identifiable by methylene blue staining) based on section-by-section comparison of our series with the series of Paxinos et al. (2007). Interpolation between multiple sections from the Paxinos et al. (2007) series was used where necessary to obtain appropriate outlines that could be superimposed on our sections (see Fig. 2). Interpolation was performed by dividing atlas sections into dorsoventral slices and sorting slices from adjacent sections systematically along the dorsoventral axis to more closely match the section orientation in our material.

Relative neuron numbers

To obtain estimates of the relative number of neurons within the pRS neuron subpopulations, three different procedures were used. In the first, we multiplied by 6 the number of marked pRS neurons compiled in every sixth 14-µm section of the 3D reconstructions (described above). This approach allowed us to determine on the basis of atlas-defined regions whether a given pRS neuron was present in the PnO or the PnC. In the second, we counted all the soma outlines that were drawn in the parasagittal 50-µm sections used for spatial distribution maps. Because these did not include atlas-derived information, we used a rostrocaudal discontinuity in the mediolateral distribution of the ipsilateral pRS neurons visible in the sagittal plane (which we operationally define as the transition from PnO to PnC; see Results) to denote whether a neuron was located in the PnO or PnC. In the third, we counted the number of visibly labeled neurons lying within the relevant region of the PRF in serial transverse 50-µm sections and used section number to estimate the location of the discontinuity described above. Because our aim was not to determine exact numbers but rather to obtain relative numbers in different neuron populations, we did not apply any corrections for potential errors from “double counting” of neurons intersected by a section plane (see Discussion).

Statistical analysis

Data analysis was performed in Excel or the statistics software SPSS (IBM). All graphs and plots were produced in SPSS. Distributions are presented as means ± standard deviations. Statistical differences in means were determined with the Mann-Whitney U-test.

RESULTS

The pRS neurons and their axons were retrogradely labeled unilaterally from the spinal C2 segment in isolated brainstem–spinal cord preparations from 26 newborn (P0) ICR mice (Fig. 1A). In 13 preparations, the white matter encompassing the VF and LF was labeled in its entirety on one side. In the other 13 preparations, retrograde labeling was restricted to one of three zones that divided the combined VF + LF into equal parts (zones 1–3, Fig. 1B–D). To ensure that the LF was labeled throughout its dorsal extent, we always extended the application site into the dorsolateral fasciculus (df, as described by Sengul et al., 2012; arrow in Fig. 1B–C) in VF + LF and in zone 3 preparations. Three VF + LF preparations and two each of the zone 1, 2, and 3 preparations were used for 3D reconstructions. Two VF + LF preparations were used for neuron size, density, and spatial distribution analyses. The remaining preparations were used for qualitative anatomical analyses and estimates of relative neuron numbers.

General spatial distribution of ipsilaterally and contralaterally projecting pRS neurons

Retrogradely labeled neurons were found in several regions of the pons, including those corresponding in the atlas of Paxinos et al. (2007) to the nucleus reticularis pontis pars oralis (PnO) and pars caudalis (PnC), the locus coeruleus (LC), the nucleus subcoeruleus (SubCA), the vestibular nuclei, and several structures and areas adjacent to these (Fig. 2; some of the retrogradely labeled neuron populations are not visible in the low-magnification images). Here we focus only on the neurons labeled retrogradely within the region corresponding to the pontine reticular nuclei (PnC and PnO) together with small numbers of neurons clearly contiguous with these and not associated with other distinct labeled neuron clusters nearby. We denote these neurons collectively as the *pRS neuron* population. In the description that follows, we describe the pRS neuron population in a series of four transverse sections moving from rostral to caudal (Fig. 2A–D), taken from a representative preparation. To provide anatomical orientation, we have superimposed boundaries of specific nuclei and axon tracts onto each section. Some of these were obtained from the intercalated methylene blue-stained sections (solid lines in Fig. 2), whereas others were transferred from the atlas of Paxinos et al. (2007; dotted lines in Fig. 2; see Materials and Methods for a detailed description of how this was done). However, we wish to emphasize that delineation of neuroanatomical structures is by its very nature subjective, particularly in regions such as the reticular formation, and should always be interpreted with caution. In other words, that a neuron is located within a drawn boundary is not sufficient evidence to prove that it resides in the delineated structure, let alone that is a functional component of that structure. We therefore use the term *presumed border* in the description below.

As shown in the most rostral section (Fig. 2A), labeled pRS neurons were located both ipsilateral and contralateral to the tracer application site, beginning at about the same rostral

level. The ipsilateral pRS neurons were located dorsolaterally within the area corresponding to the PnO. The contralateral pRS neurons were located ventrolaterally, having a center of density just inside the presumed PnO border, with some found on either side of this border.

Moving caudally (Fig. 2B), the ipsilateral pRS neuron population broadened dorsoventrally so that it occupied the whole lateral half of the PnO. Some ipsilateral pRS neurons were located outside the presumed ventrolateral border of the PnO, close to and sometimes among the labeled axons of the rubrospinal (rs) tract (Fig. 2B). At this level, a few labeled neurons were also found within the ipsilateral subcoeruleus nucleus, alpha part (SubCA). These cannot be seen in the low-magnification image but were visible at higher magnification in the microscope. As defined above, we did not consider these labeled neurons to be part of the pRS neuron population because they clearly made up a separate, distinct group. The contralateral pRS neuron population at this level maintained a more restricted location in the ventrolateral corner of the PnO, with some neurons located just outside the putative ventrolateral border and spreading into the ventral nucleus of the lateral lemniscus (VLL).

Moving farther caudally into the PnC (Fig. 2C), the ipsilateral pRS population shifted ventrally and medially and was more clearly separated from the labeled neurons in the dorsal part of the SubCA. Contralateral pRS neurons at this level were substantially less numerous and more faintly labeled (they are more easily seen in the enhanced inset).

At the most caudal level (Fig. 2D), the ipsilateral pRS neuron population remained within the putative border of the PnC but shifted slightly medially. The contralateral pRS population on the other hand shifted laterally outside of the putative PnC border into the region containing the superior olive (SO) and the intermediate reticular nucleus (IRt). Because the neurons involved maintained contiguity with the contralateral pRS population at more rostral levels and did not generate or associate with a separate group of labeled neurons (see 3D reconstructions below), we consider them to be part of the contralateral pRS population. We defined operationally the border between pons and medulla, which inherently delineates the caudal limit of the pRS neuron population, as the level where labeled raphespinal neurons appeared (not visible in the sections shown here).

Detailed topography of the ipsilaterally and contralaterally projecting pRS neurons

The topography of the ipsilateral and contralateral pRS neuron subpopulations and their spatial relationship was quantified in the two parasagitally sectioned preparations that were used for spatial distribution plots. The plot in Figure 3A shows the mediolateral positions of ipsilateral (magenta circles) and contralateral (green circles) pRS neurons along the rostrocaudal axis, in effect presenting a ventral view of the pRS neuron population. The two subpopulations have been placed on the same side to illustrate the degree of overlap and segregation. As shown, the ipsilateral pRS neuron subpopulation occupied a more medial position than its contralateral counterpart, at all rostrocaudal levels. This view also shows that within the ipsilateral subpopulation a distinct mediolateral shift occurred midway along the rostrocaudal axis (at approximately 400 μm from the caudal limit of the PRF). The average distance from the midline of the pRS neurons located above and below this shift differed by 165 μm. In comparison with the regions defined in Paxinos et al. (2007), the location of this discontinuity in mediolateral position along the rostrocaudal axis appears to

relate to the transition from the PnO to the PnC. In the descriptions that follow, we provisionally equate the pRS subpopulations above and below this discontinuity to those within the PnO and PnC, respectively.

The plot in Figure 3B shows the dorsoventral positions of ipsilateral and contralateral pRS neurons along the rostrocaudal axis, in effect presenting a side view of the pRS neuron population. This view shows clearly the more dorsal position of the ipsilateral pRS neuron subpopulation relative to its contralateral counterpart as well as the gradual dorsal to ventral shift of each population moving from rostral to caudal. This dorsal to ventral shift results from the gradual curvature of the pRS neuron population as it follows the natural curvature of the longitudinal axis of the pons.

The plot in Figure 3C shows the mediolateral positions of ipsilateral and contralateral pRS neurons along the dorsoventral axis, in effect presenting an axial view of the pRS neuron population. This view shows a relatively sharp segregation between the ipsilateral and the contralateral pRS populations, which was not as evident in Figure 3A or B because the line of segregation is angled with respect to both the frontal and the sagittal planes. This view also shows that each population is sharply delineated eccentrically to the line of segregation, mediodorsally and lateroventrally for the ipsilateral and contralateral pRS populations, respectively. Altogether the data indicate that, despite a partially overlapping spatial distribution in the PnO and PnC regions, the ipsilateral and contralateral pRS neurons have characteristic locations with the ipsilateral subpopulation occupying a more medial and dorsal position.

Estimates of relative pRS neuron numbers and differential targeting of pRS axons to the spinal white matter

As described in Material and Methods, to estimate the relative number of ipsilateral and contralateral pRS neurons, we used three different approaches to count neurons in preparations that had received tracer application in the VF + LF. Counting individually marked pRS neurons in 3D-reconstructed brainstems (n = 3) permitted correlation to the domains of the PnO and PnC as defined by Paxinos et al. (2007). Counting pRS neuron soma outlines in the position plots from the serially and parasagittally sectioned preparations used for Figure 3 (n = 2) allowed us to identify pRS neurons as located rostral or caudal to the mediolateral discontinuity described in the previous section. Counting visibly labeled pRS neurons in serially and transversely sectioned preparations (n = 4) required using the midway point within the rostrocaudal extent of the ipsi-pRS neuron population as the division between the same rostral and caudal regions defined by the mediolateral discontinuity. Estimates from all three approaches indicated that the numbers of pRS neurons were clearly larger on the ipsilateral side than on the contralateral side throughout the rostrocaudal extent of the pons (Fig. 3D, Table 2). Moreover, the ipsilateral pRS neuron population was roughly equally divided between the PnO and PnC, whereas the contralateral population was clearly more concentrated in the PnO than in the PnC (Fig. 3D, Table 2). Hence, the ipsilateral predominance of pRS neurons was more obvious caudally within the region corresponding to the PnC.

Descending pRS axons entered the spinal cord along a broad mediolateral swath of white matter. To examine the possibility of an internal organization of the pRS neurons related to initial spinal axon trajectories, in 13 preparations, we restricted labeling to one of three roughly equal zones of the combined VF + LF (zones 1–3; Fig. 1 and cartoons at the bottom of Figure 4). The three preparations shown in Figure 4 were used for imaging purposes only. Four additional preparations (zone 1, n = 2; zones 2 and 3, n = 1 each) were used for direct cell counting from serial transverse sections as described above. The remaining six preparations (zones 1–3, n = 2 each) were 3D reconstructed (Fig. 5) and counts were obtained as described above. Zones 1–3 were not intended to match any traditional subdivisions of the white matter, but our assessment indicates that zone 1 contains only VF fibers, zone 3 contains mostly LF fibers, and zone 2 contains parts of both, but probably more VF than LF.

Tracing selectively from each zone resulted in distinct, reproducible patterns of labeling within the pRS neuron populations (Table 2, Figs. (4 and 5)). Zone 1 (column A in Fig. 4) labeled many ipsilateral but few contralateral pRS neurons, zone 2 (column B in Fig. 4) labeled ipsilateral and contralateral pRS neurons in proportions similar to their numbers in VF + LF preparations, whereas zone 3 (column C in Fig. 4) labeled few ipsilateral but many contralateral pRS neurons. The zone-related distribution of ipsilateral pRS neurons showed a clear differentiation along the rostrocaudal axis. Zone 1 labeled relatively more ipsilateral pRS neurons in the PnC than the PnO (more evident in Table 2 than in Fig. 4), zone 2 labeled them about equally in the PnO and PnC (roughly in proportion to their numbers in VF + LF labeled preparations), whereas zone 3 labeled hardly any ipsilateral pRS neurons in the PnC. There was less rostrocaudal differentiation of contralateral pRS neuron labeling as a function of zone, except that zone 1 only very rarely labeled any contralateral pRS neurons within their most prevalent location in the ventrolateral region of the PnO. These relationships can also be appreciated in the 3D reconstructions shown in Figure 5.

We note that in Table 2 the numbers of pRS neurons labeled from the different zones do not add up to the numbers obtained when labeling the VF + LF in its entirety. The most likely explanation is that the cuts made to label the different zones overlapped slightly from preparation to preparation, and, where axon density is high (for example, at the transition from zone 1 to zone 2), even minor overlap could lead to labeling of large numbers of “unintended” axons. Thus, we do not emphasize the neuron numbers here but rather focus on the very clear correlation between topography within the pRS neuron populations and mediolateral location of the descending axons.

To summarize, the number of ipsilateral pRS neurons was on average approximately three times the number of contralateral pRS neurons, and this relative predominance was particularly apparent in the PnC. The majority of ipsilateral pRS neurons in the PnO and PnC was labeled from the medial part of the VF (zone 1), but substantial numbers were labeled from the lateral part of the VF (zone 2). In contrast, the majority of contralateral pRS neurons in both PnO and PnC was labeled from the LF (zone 3).

Regional differences in pRS neuron soma size and density

Examination of labeled ipsilateral and contralateral pRS neurons in low-magnification parasagittal sections (Fig. 6A and B, respectively) suggests the presence of regional differences in soma sizes in each population. As shown in Figure 6C–E, measurements of soma size demonstrated differential distributions along the different axes. In the PnO (above the dotted line in Fig. 6A,B), average soma size was similar in the two pRS neuron populations (grand averages: ipsilateral, 178.7 ± 81.7 μm^2; contralateral, 181.3 ± 67.6 μm^2) and relatively constant along the rostrocaudal axis (Fig. 6C). By contrast, in the PnC (below the dotted line in Fig. 6A,B), average soma size was noticeably larger in the ipsilateral population (accompanied by increased variability; 235.0 ± 102.2 μm^2) and smaller in the contralateral population (150.5 ± 49.8 μm^2). Along the mediolateral axis (Fig. 6D), average soma size varied less. Finally, along the dorsoventral axis (Fig. 6E), there was a clear tendency for increasing soma size in the ipsilateral population moving from dorsal to ventral, although there was no clear trend in the contralateral population.

The regional differences in soma size along the ros trocaudal axis prompted us to assess whether this was correlated to similar differences in pRS neuron density (Fig. 7). Neuron density was obtained directly from the position plots shown in Figure 3 and averaged in the transverse plane (thick vertical bars in graph of Fig. 7). For both the ipsilateral and the contralateral pRS neuron populations, the density was clearly lowest in the most rostral reaches of the PnO, whereas for the remainder of the PnO and for the PnC it was variable without any clear tendency along the rostrocaudal axis.

Differential rostrocaudal distribution of putative GABAergic neurons intercalated among the pRS neurons

In a separate study, we are assessing the differential gene expression profiles of the pRS neuron subpopulations, including their neurotransmitter phenotypes. As part of this effort, we have examined whether any pRS neurons might be GABAergic by labeling them in transgenic mice that express reporter constructs driven by the GAD67 promoter. In neither the GAD67 GFP nor the GIN transgenic mouse strains were any pRS neurons GFP positive. However, we did observe a differential distribution of putative GABAergic neurons in GAD67 GFP and GIN mice as they relate to the pRS neuron population, which we report here (Fig. 8). In the GAD67 GFP mouse, numerous putative GABAergic interneurons were found in the PnO and PnC, and these were interspersed among the ipsilateral and contralateral pRS neurons. In the GIN mouse, putative GABAergic interneurons were found nearly exclusively in the PnC and, therefore, interspersed primarily among ipsilateral pRS neurons because of the paucity of contralateral pRS neurons. Thus, these two different subpopulations of putative GABAergic neurons were differentially distributed in the PnO and PnC, a finding that could relate to the local circuitry operating on the pRS neurons in these two regions.

Trajectories of pRS axons in the brainstem

Retrograde labeling with conjugated dextrans also reveals information about the trajectories of the labeled pRS axons. As shown in the examples illustrated in Figure 9, we sectioned a set of labeled preparations in specific planes designed to align with pRS axon trajectories

within the brainstem. These planes were deduced from the material that we had sectioned in the transverse, horizontal, and sagittal planes.

As a rule, the axons of the ipsilateral pRS neurons (Fig. 9A–D) projected initially in a mediodorsal direction and followed quite strictly the natural transverse plane of the pons (the plane changes gradually along the rostrocaudal axis in keeping with the curvature of the pons). As they approached the MLF, ipsilateral pRS axons made a sharp, approximately 90 ° turn toward the spinal cord (arrowheads in Fig. 9B–D) and formed a loosely organized axon bundle, the densest part of which adjoined the MLF. In confocal stacks from different parasagittal or transverse planes through the PnO (Fig. 9B) or the PnC (Fig. 9A,C,D), it can be appreciated that, before turning to descend, many ipsilateral pRS axons coursed all the way to their most medial position while maintaining the same rostrocaudal level (best illustrated by the color code for depth in Fig. 9C,D).

The axons of the contralateral pRS neurons located in the PnO had a trajectory similar to that of the ipsilateral pRS axons but with some notable differences at the start. They initially projected in a dorsomedial direction and, upon reaching a specific dorsal point, turned abruptly toward the midline (Fig. 9E). After they crossed the midline, they joined a forest of labeled axons in this area. Presumably, they here turn in a caudal direction, but the density of labeled axons prevented us from following individual axons. The entire initial axonal trajectory of the contralateral pRS axons has been captured in Figure 9E with at least one axon visible throughout the trajectory up to the caudal turn. The trajectory can also be appreciated in Figures 2C and 7C, even though the section planes used here were not adapted to show it in its entirety. The few contralateral pRS axons originating in the PnC were too weakly labeled to follow with certainty.

DISCUSSION

General overview of results

Through selective retrograde labeling, we have characterized the internal organization of the pRS neuron population, with particular emphasis on the spatial relationship between the ipsilaterally and the contralaterally projecting subpopulations and on the topographical relationship to axon trajectories and initial spinal funicular destinations. Our salient findings are that 1) ipsilateral pRS neurons are threefold more numerous than contralateral pRS neurons; 2) ipsilateral pRS neurons are equally divided between the PnO and the PnC, whereas contralateral pRS neurons are most prevalent within the PnO; 3) ipsilateral and contralateral pRS neuron populations are spatially segregated; 4) ipsilateral and contralateral pRS neurons exhibit opposite rostrocaudal gradients in soma size; 5) two different subsets of putative GABAergic interneurons are intercalated among pRS neurons but differentially distributed between the PnO and PnC; 6) ipsilateral and contralateral pRS neurons have distinct axon trajectories within the brainstem; and 7) ipsilateral and contralateral pRS axons target the ventral and lateral spinal white matter differentially and in opposing gradients as they enter the spinal cord, with ipsilateral pRS axons more concentrated medially (in the VF and ventral part of LF) and contralateral pRS axons more concentrated laterally (dorsal part of LF). Additional targeting is seen within the ipsilateral pRS axon population, with ipsilateral pRS axons originating from the PnC and the PnO coursing, respectively, medially

and laterally within their overall gradient. The principal features of organization and axon trajectory are summarized in Figure 10.

Technical considerations

Determining pRS neuron distributions and relative numbers with retrograde labeling—Identifying neurons in the PRF as pRS neurons requires demonstrating that they project to the spinal cord. Retrograde labeling, as done here, is a practical way to ensure this. There are limitations to retrograde labeling techniques that can affect the assessment of neuron distribution and number, however. Earlier studies have shown that, despite providing dependable and reproducible patterns of labeling in the central and peripheral nervous systems, retrograde labeling with conjugated dextrans typically is not 100% efficient and therefore underestimates the total number of neurons within a given labeled population (see, for example, Stokke et al., 2002, who demonstrated suboptimal retrograde labeling of spinal interneurons). At least one report, with regard to the lamprey, indicates that retrograde labeling of reticulospinal neurons with conjugated dextrans may be biased toward larger axon caliber (Brodin et al., 1988). Labeling bias of this type is important, because insufficient or absent labeling of a projection neuron subpopulation would clearly misrepresent the real picture. Of relevance in this regard is our observation that the more caudal contralateral pRS neurons were consistently labeled with weaker intensity than other pRS neurons. We have ruled out that this weak labeling is artifactual through an extensive series of control experiments to test for indirect contamination from the application site to axons not intended to be labeled (not shown), and because these neurons are among the closest to the application site it seems unlikely that axon length is a decisive factor. We thus have no good explanation for why the labeling was consistently weaker in this particular pRS neuron subpopulation.

Neuron counts obtained from sections are subject to potential counting errors, which can either overestimate or underestimate neuron number, depending on circumstances (Abercrombie, 1946; Hendry, 1976; Williams and Rakic, 1988). This can be overcome to a large extent by stereological methods (Gundersen et al., 1988; Williams and Rakic, 1988; West, 1993), which we did not employ. Nor did we use correction factors to minimize the effect of systematic counting errors because our principal interest has been to obtain relative rather than absolute neuron counts. Although counting errors from sectioning could affect the two pRS neuron subpopulations differentially because of their soma size differences, it is unlikely that this kind of error could generate the threefold difference observed, especially because a similar proportion was obtained in counts from 14-μm sections and 50-μm sections. We are therefore confident in our description of the regional segregation and relative numbers of the two pRS neuron subpopulations. Taken at face value, our estimates indicate that there are approximately 900 pRS neurons in total on each side of the PRF, of which about one-fourth are contralaterally projecting. It should be noted that Liang et al. (2011) report substantially more pRS neurons in the adult mouse, on the order of 6,500 on each side, using Fluorogold as tracer and 96 hours of in vivo tracer transport time. They also caution that their counts of retrogradely labeled neurons should be considered only as estimates. They, like us, did not use stereological methods or counting correction factors. It

remains to be determined what the discrepancy between neonatal and adult counts represents.

Ambiguity of cytoarchitectonics—As we have pointed out from earlier studies in which we have compared retrogradely labeled bulbospinal neuron populations to cytoarchitectonic divisions of the hindbrain (Díaz et al., 2003), the mapping of cytoarchitectonic boundaries is by nature subjective and can vary from investigator to investigator and even from study to study by the same investigator, especially if different section planes are used. Thus, we believe that cytoarchitectonic boundaries should be used with great caution. Here, we have transferred boundaries of the PnO and PnC, and of other structures in their vicinity, from the atlas generated by Paxinos et al. (2007), aligning them with landmarks visible in our material. Because we have not used Nissl staining as in that atlas, but rather methylene blue staining, which provides less cytoarchitectonic detail, and because methylene blue-stained sections were intercalated between sections stained for the conjugated dextran tracers, section alignment introduces additional subjective interpretation. Despite these caveats, our material indicates that coherent clusters of pRS neurons are located largely but not completely within the putative boundaries of the PnO and PnC. We suggest that boundary transgressions, to the extent that they do not obviously encroach on other well-defined neuron clusters nearby, are of minimal functional significance. It seems most likely that anatomical coherence of retrogradely labeled neuron populations is a direct result of early patterning mechanisms that define axon projection pathway and to some extent synaptic connectivity (for discussion see Diaz et al., 2003), such that this coherence should be considered a stronger indication of common identity than should compliance with subjectively defined boundaries.

Internal organization of the pRS neuron population

Comparison with other retrograde tracing studies in the mouse and rat—Several previous retrograde tracing studies have demonstrated projections from the PRF to the spinal cord in the mouse and rat, ranging from embryonic to adult stages (mouse: Auclair et al., 1999; Vanderhorst and Ulfhake, 2006; Liang et al., 2011, 2015; rat: Basbaum and Fields, 1979; Satoh, 1979; Watkins et al., 1980, 1981; Leong et al., 1984a,b; Newman, 1985; Jones and Yang, 1985; Nudo and Masterton, 1988; Rye et al., 1988; Shen et al., 1990; Masson et al., 1991; Lakke, 1997; Auclair et al., 1999; Reiner et al., 2008; Huma et al., 2014). Only three of these studies combined unilateral tracer application with contralateral spinal cord hemisection to ensure unilateral tracing so that the laterality of projections could be unequivocally documented (Basbaum and Fields, 1979; Auclair et al., 1999; Vanderhorst and Ulfhake, 2006), as we have done here. In eight other studies, in the adult mouse or rat, unilateral applications were made but not combined with contralateral lesions to ensure unilateral tracing (Watkins et al., 1980, 1981; Newman, 1985; Nudo and Masterton, 1988; Reiner et al., 2008; Liang et al., 2011, 2015; Huma et al., 2014). These studies will receive additional attention below. In the remaining studies, the laterality of retrograde tracing is inherently questionable.

Nearly all of the studies cited above have shown that both the PnC and the PnO project to the spinal cord; a few authors describe projections only from the PnC. Liang et al. (2011)

also distinguish the PnV (ventral pontine reticular nucleus), containing a minor population of reticulospinal neurons, which may in fact be the most rostral part of the medullary gigantocellular nucleus, potentially misconstrued as having a pontine location because of mismatch between coronal sections of the adult brain and the planes of rhombomere boundaries (see below). With regard to laterality, Basbaum and Fields (1979), Auclair et al. (1999), Vanderhorst and Ulfhake (2006), and Huma et al. (2014) all report an ipsilateral predominance in the projection of pRS neurons throughout the PRF, including both the PnO and the PnC. Newman (1985) concurs, with a distinction between the PnC (his RPoC) pars alpha and beta, which project, respectively, with contralateral and ipsilateral predominance, and between the PnO (his RPoO) medialis and lateralis, which project, respectively, with a weak ipsilateral predominance and no lateral bias. Because RPoC pars beta and RpoO medialis correspond to the more dorsal and medial regions of the PnC and PnO, respectively, the ipsilateral predominance of pRS neurons in these specific regions reported by Newman (1985) correlates well with our results, as does the contralateral predominance of pRS neurons in the RPoC pars alpha. Nudo and Masterton (1988) also show a marked ipsilateral predominance in the pRS projection but illustrate only one level in the PRF, evidently from the PnC. Watkins et al. (1980) report an ipsilateral predominance, but, because their tracer applications were targeted to the dorsolateral funiculus with the aim of retrogradely labeling the raphespinal projection, only relatively few pRS neurons were labeled, in the most ventral region of the PRF. Using the same dorsolateral funiculus-targeted tracer applications, Watkins et al. (1981) report bilateral labeling in PnC and contralateral labeling in PnO, again with only few pRS neurons labeled. In contrast to these studies, Reiner et al. (2008) report equal numbers of ipsilateral and contralateral pRS neurons regardless of whether injections were made at cervical, thoracic, or lumbar levels, and Liang et al. (2011) report a substantial contralateral predominance of projections from the PnO following tracer injections into the cervical spinal cord, although they do report an ipsilateral predominance for the PnC. Liang et al. (2015) present images that suggest an ipsilateral predominance in the PnO following tracer injections in the lumbar spinal cord. Because a large proportion of pRS neurons in the PnO projects very medially (in the ipsilateral zone 1), it seems plausible that the contralateral predominance of the PnO projection reported by Liang et al. (2011) following cervical tracer injections and the nearly symmetrical laterality reported by Reiner et al. (2008) might have arisen from contamination of medially located axons on the side contralateral to the injection. This would label ipsilaterally projecting pRS neurons in the PnO contralateral to the tracer injection site, which would then be misinterpreted as projecting contralaterally. An additional sign of such potential contamination is the much more symmetrical labeling of neurons in the ventral portion of the nucleus subcoeruleus reported by Liang et al. (2011) than that reported by Vanderhorst and Ulfhake (2006) and here. The discrepancies in laterality underscore the importance of using lesions in conjunction with tracer injections if the aim of retrograde labeling is to determine the laterality of axon descent while avoiding the complicating issues of contralateral tracer contamination and commissural collateralization of axons within the spinal cord.

Comparison to retrograde tracing studies in other mammals—Although an exhaustive description of the literature on bulbospinal projections in nonrodent mammals is beyond the scope of this discussion, it is worth noting that the pRS projection has been

described in a variety of mammalian species, particularly the opposum (Martin et al., 1979, 1988; Cabana and Martin, 1984), cat (Nyberg-Hansen, 1965; Petras, 1967; Basbaum and Fields, 1979; Tohyama et al., 1979; Holstege et al., 1979; Hayes and Rustioni, 1981; Mitani et al., 1988; Rice et al., 2010), and nonhuman primates (Carlton et al., 1985; Sakai et al., 2009). In general, these studies indicate that asymmetry with ipsilateral predominance of the pRS projection is a conserved feature, although discrepancies regarding laterality also exist in this literature.

Although we have focused here on the pRS neuron populations in the core of the PRF that relate directly to the stimulation sites that we identified in our previous study (Sivertsen et al., 2014), it is also important to note that descending pathways from the pontine reticular formation and the pons in general are functionally heterogeneous. Several specific pathways to the spinal cord have been identified that regulate such diverse functions as respiration, nociception, micturition, defecation, sexually triggered glandular secretion, and noradrenergic modulation (for review see Holstege and Kuypers, 1982; Holstege, 1991, 1998). In a separate publication, we will present an atlas of bulbospinal neurons in the neonatal mouse in which many of these functionally characterized neuron groups are individually mapped.

Relationship to developmental patterning—By comparison with our earlier study of reticulospinal and vestibulospinal neurons in mouse and rat embryos, it seems quite clear that the pRS neurons are located in the rostrocaudal domain that derives from rhombomeres (r) 1–4 (Auclair et al., 1999). In that earlier study, we also noted the development of a distinct discontinuity in the shape of the ipsilateral and contralateral pRS neuron populations, located at the transition from r2 to r3. Thus, we propose that this discontinuity in embryos corresponds to the rostrocaudal discontinuity in the mediolateral location of ipsilateral pRS neurons reported here, which we have operationally defined as the transition from PnO to PnC. This would mean that the PnO derives from r1–2 and the PnC derives from r3–4. The rhombomere-related discontinuity becomes apparent about 1 day after pRS axons reach the spinal cord (Auclair et al., 1999), indicating that it originates through cell aggregation imposed on initially more evenly distributed neurons, in other words, a relatively late feature of patterning. By contrast, a differential location of ipsilateral and contralateral pRS neuron subpopulations in the transverse plane is evident as early as the pRS neurons can be retrogradely labeled from the spinal cord (Auclair et al., 1999), suggesting that this feature of patterning originates early, likely because the two subpopulations originate from different dorsoventral progenitor domains.

Relationship to function—The numerical predominance of ipsilateral vs. contralateral pRS neurons is significant relative to our previous report on the synaptic inputs from pRS neurons to spinal MNs (Sivertsen et al., 2014). In that study we found both an ipsilateral and a contralateral projection from the PRF to MNs, but the ipsilateral projection transmitted more faithfully and appeared to be more direct. Accordingly, we suggest that this difference in functional connectivity is due at least in part to differences in the spinal targets of the ipsilateral and contralateral pRS neurons. Ipsilateral pRS neurons evidently innervate MNs either directly or through few intermediate INs, whereas contralateral pRS neurons innervate

primarily INs. How this relates to behavior is not yet clear. The PnC is involved in postural control and is a main relay for auditory-stimulus-elicited startle reactions (Davis et al., 1982; Femano et al., 1984; Yeomans and Frankland, 1996). The latter generates widespread and bilateral activation of head, neck, trunk, and limb musculature, whereas the former can involve more selective activation of muscles. The PnO overlaps the mesopontine tegmental anesthesia area, which when pharmacologically activated exerts widespread spinal anesthesia and atonia (Reiner et al., 2008). Anterograde tracing in several mammalian species, including the mouse, has shown that axons from PnO and PnC terminate throughout the length of the spinal cord, and differential retrograde tracing from multiple spinal levels suggests a high degree of rostrocaudal collateralization by individual pRS axons (selected studies in rodents: Sirkin and Feng, 1987; Reiner et al., 2008; Liang et al.; 2015). As in the cat (Matsuyama et al., 1993, 1999), pRS axon terminals in rodents are particularly focused on the ipsilateral laminae VII and VIII, which are known to contain premotor interneurons, and are also found in the contralateral cord. Given the difficulty of distinguishing terminals derived from individual axons and the diversity of spinal interneurons that populate the regions of termination, a more comprehensive functional characterization of the spinal targets of the PnO and PnC and their ipsilateral and contralateral pRS subpopulations is warranted.

Differences in pRS soma size can be related to several functional characteristics, including density of synaptic input, input resistance and its effects on synaptic integration, susceptibility to electrical stimulation, thickness and conduction velocity of axons, and number of axon terminal branches and synaptic contacts maintained on target neurons. Thus, it is likely that the regional differences that we observed in soma size reflect functional heterogeneity within the pRS population.

The differential distribution between PnO and PnC of the two subpopulations of putative GABAergic interneurons defined by the GAD67 GFP and GIN transgenic mouse lines suggests that local circuitry involved in information processing within the more rostral and caudal pRS neuron populations may also differ. GABAergic interneurons genetically labeled in the GIN line comprise multiple functional subtypes within the somatostatin-expressing subclass (Halabisky et al., 2006), whereas those genetically labeled in the GAD67 GFP line comprise a larger and more varied set that includes somatostatin-, parvalbumin-, and calretinin-expressing interneurons (Tamamaki et al., 2003). Selective optogenetic manipulation of different subsets of GABAergic interneurons could be used in the future to test the functional significance of differentially distributed GABAergic neurons interspersed among the pRS neurons.

Topography of supraspinal axon trajectories and initial spinal funicular projections

Characterizing supraspinal axon trajectories and initial spinal funicular destinations is important for two reasons. First, it provides clues about how axons from different neuron populations navigate toward their targets during development. Second, it provides information that can increase the precision of electrical stimulation, photostimulation, and lesions in physiological studies of the descending effects of specific axon populations.

The trajectories of pRS axons within the brainstem and their initial funicular targeting in the spinal white matter clearly differ between the ipsilateral and the contralateral pRS neuron subpopulations. Ipsilaterally projecting pRS axons course dorsally toward the midline, parallel to each other in a broad swath matching the rostrocaudal extent of their parent somata, before turning to descend in a largely medial location that overlaps but is not restricted to the MLF. The overall trajectory is very similar to that described for individual pRS neurons in the PnC in the adult rat (Lingenhohl and Friauf, 1994). By contrast, contralaterally projecting pRS axons follow a more tortuous path to their descending turning point, starting in a dorsomedial direction and then veering ventrally before crossing the midline. They cross the midline in a rostrocaudally narrower bundle relative to the ipsilaterally projecting axons. Upon turning to descend, the ipsilaterally and contralaterally projecting axons tend to take up more medial and lateral positions, respectively, and, as they reach the spinal cord, they distribute with opposite gradients within the VF and LF.

Huma et al. (2014) also aimed to assess, in the adult mouse, the white matter trajectories of bulbospinal neurons, including those in the PRF. They combined unilateral lumbar injection of one retrograde tracer with ipsilateral injection of another retrograde tracer in either the MLF or the caudal ventrolateral medulla. They report a predominantly medial targeting of ipsilateral pRS axons originating from both the PnO and the PnC and a predominantly lateral targeting of contralateral pRS axons originating from the PnC, similar to what we report for the neonate. However, they report that contralateral pRS neurons in the PnO project predominantly medially, which does not fit with our results. Because they did not ensure unilateral labeling with a contralateral lesion, there again is a possibility that this discrepancy arises from contamination of the MLF on the side opposite the injection.

It is important to keep in mind that our labeling has been performed from the high cervical spinal cord and thus labels pRS neurons regardless of how far their axons project down the cord. Much additional work remains to determine whether pRS neurons are also organized according to how far they project and what targets they innervate in the spinal cord.

Our description also provides a tool that can facilitate the physiological assessment of synaptic connections between pRS neurons and spinal neuron targets, by indicating where lesions can be placed to restrict impulse traffic to identifiable axon subpopulations. For example, by making a midline lesion in the pons together with a lesion in the upper cervical cord sparing zone 1, transmission of impulses elicited by stimulation of the PRF would be strongly biased toward ipsilateral pRS neurons in the PnC, whereas an upper cervical lesion sparing zone 3 would strongly bias toward ipsilateral pRS neurons in the PnO.

Future directions

We are currently pursuing two lines of research to characterize the pRS neurons further. The first of these involves neurotransmitter phenotyping. In our study of synaptic connections from pRS neurons onto spinal MNs, we used calcium imaging that readily reveals excitatory connections (Sivertsen eal., 2014). However, there is evidence that activation of spinal MNs by electrical stimulation within the ipsilateral PnC can be inhibited by concomitant stimulation within the contralateral PnC (Femano et al., 1984). Thus, we are performing a variety of assays to establish the neurotransmitters used by the ipsilateral and contralateral

pRS neuron subpopulations. The second line of research is focused on developmental patterning. Because the ipsilateral and contralateral pRS neuron subpopulations appear to derive from different dorsoventral domains in the developing hindbrain, we are carrying out fate-mapping experiments to determine their transcription factordefined progenitor domains of origin. This will provide information about how the two subpopulations become specified to differentiate their specific characteristics as well as an avenue for transgenic manipulation, including the use of optogenetic tools for more selective physiological studies.

ACKNOWLEDGMENTS

We thank Kobra Sultani for technical assistance with the mouse colony, Marian Berge Andersen for cryostat sectioning, and Sveinung Lillehaug for help with Neurolucida reconstructions.

Grant sponsor: Norwegian Research Council and the University of Oslo (to J.C.G.); Grant sponsor: South-East Norway Regional Health Authority (to M.-C.P.).

Abbreviations

4V	fourth ventricle
5N	motor trigeminal nucleus
5TT	motor trigeminal nucleus, tensor tympani part
6N	abducens nucleus
Bar	Barrington’s nucleus
DC	dorsal cochlear nucleus
DMTg	dorsomedial tegmental area
DRC	dorsal raphe nucleus, caudal part
DTgP	dorsal tegmental nucleus, pericentral part
IRt	intermediate reticular nucleus
KF	Kölliker-Fuse nucleus
LC	locus coeruleus
LDTg	laterodorsal tegmental nucleus
LVe	lateral vestibular nucleus
mlf	medial longitudinal fascicle
MnR	median raphe nucleus
MVeMC	medial vestibular nucleus, magnocellular part
MVePC	medial vestibular nucleus, parvicellular part
PCRtA	parvicellular reticular nucleus, alpha part
PMnR	paramedian raphe nucleus
Pn	pontine nuclei

PnC	pontine reticular nucleus, caudal part
PnO	pontine reticular nucleus, oral part
Pr5	principal sensory trigeminal nucleus
pRS	pontine reticulospinal
RIP	raphe interpositus nucleus
Rpa	raphe pallidus nucleus
rs	rubrospinal tract
RtTg	reticulotegmental nucleus of the pons
SO	superior olive
SpVe	spinal vestibular nucleus
Su5	supratrigeminal nucleus
SubCA	subcoeruleus nucleus, alpha part
SubCD	subcoeruleus nucleus, dorsal part
SuVe	superior vestibular nucleus
Tz	trapezoid body
VeCb	vestibulocerebellar nucleus
VLL	ventral nucleus of the lateral lemniscus
Vtg	ventral tegmental nucleus
X	nucleus X

LITERATURE CITED

Abercrombie M. Estimation of nuclear population from microtome sections. Anat Rec. 1946; 94:239–247. [PubMed: 21015608]

Auclair F, Marchand R, Glover JC. Regional patterning of reticulospinal and vestibulospinal neurons in the hindbrain of mouse and rat embryos. J Comp Neurol. 1999; 411:288–300. [PubMed: 10404254]

Baker SN. The primate reticulospinal tract, hand function and functional recovery. J Physiol. 2011; 589:5603–5612. [PubMed: 21878519]

Basbaum AI, Fields HL. The origin of descending pathways in the dorsolateral funiculus of the spinal cord of the cat and rat: further studies on the anatomy of pain modulation. J Comp Neurol. 1979; 187:513–531. [PubMed: 489790]

Brodin L, Grillner S, Dubuc R, Ohta Y, Kasicki S, Hokfelt T. Reticulospinal neurons in lamprey: transmitters, synaptic interactions and their role during locomotion. Arch Ital Biol. 1988; 126:317–345. [PubMed: 2904246]

Cabana T, Martin GF. Developmental sequence in the origin of descending spinal pathways. Studies using retrograde transport techniques in the North American opossum (*Didelphis virginiana*). Brain Res. 1984; 317:247–263. [PubMed: 6478250]

Carlton SM, Chung JM, Leonard RB, Willis WD. Funicular trajectories of brainstem neurons projecting to the lumbar spinal cord in the monkey (*Macaca fascicularis*): a retrograde labeling study. J Comp Neurol. 1985; 241:382–404. [PubMed: 4086662]

Cepeda-Nieto AC, Pfaff SL, Varela-Echavarria A. Homeodomain transcription factors in the development of subsets of hindbrain reticulospinal neurons. Mol Cell Neurosci. 2005; 28:30–41. [PubMed: 15607939]

Davis M, Gendelman DS, Tischler MD, Gendelman PM. A primary acoustic startle circuit: lesion and stimulation studies. J Neurosci. 1982; 2:791–805. [PubMed: 7086484]

Diaz C, Glover JC, Puelles L, Bjaalie JG. The relationship between hodological and cytoarchitectonic organization in the vestibular complex of the 11-day chicken embryo. J Comp Neurol. 2003; 457:87–105. [PubMed: 12541327]

Drew T, Prentice S, Schepens B. Cortical and brainstem control of locomotion. Prog Brain Res. 2004; 143:251–261. [PubMed: 14653170]

Femano PA, Schwartz-Giblin S, Pfaff DW. Brain stem reticular influences on lumbar axial muscle activity. I. Effective sites. Am J Physiol. 1984; 246:389–395.

Glover JC. Retrograde and anterograde axonal tracing with fluorescent dextrans in the embryonic nervous system. Neurosci Protoc. 1995; 30:1–13.

Glover JC. Development of specific connectivity between premotor neurons and motoneurons in the brain stem and spinal cord. Physiol Rev. 2000; 80:615–647. [PubMed: 10747203]

Gundersen HJ, Bendtsen TF, Korbo L, Marcussen N, Moller A, Nielsen K, Nyengaard JR, Pakkenberg B, Sorensen FB, Vesterby A. Some new, simple and efficient stereological methods and their use in pathological research and diagnosis. APMIS. 1988; 96:379–394. [PubMed: 3288247]

Halabisky B, Shen F, Huguenard JR, Prince DA. Electrophysiological classification of somatostatin-positive interneurons in mouse sensorimotor cortex. J Neurophysiol. 2006; 96:834–845. [PubMed: 16707715]

Hayes NL, Rustioni A. Descending projections from brainstem and sensorimotor cortex to spinal enlargements in the cat. Single and double retrograde tracer studies. Exp Brain Res. 1981; 41:89–107. [PubMed: 6162664]

Hendry IA. A method to correct adequately for the change in neuronal size when estimating neuronal numbers after nerve growth factor treatment. J Neurocytol. 1976; 5:337–349. [PubMed: 939967]

Holstege, G. Descending motor pathways and the spinal motor system. Limbic and non-limbic components. In: Holstege, G., editor. Progr Brain Res. Vol. 87. Elsevier; Amsterdam: 1991. p. 307-421.Role of the forebrain in sensation and behavior

Holstege G. The emotional motor system in relation to the supraspinal control of micturition and mating behavior. Behav Brain Res. 1998; 92:103–109. [PubMed: 9638952]

Holstege,, G. The periaqueductal gray controls brainstem emotional motor systems including respiration. In: Holstege, G.; Beers, CM.; Subramanian, HH., editors. Prog Brain Res. Vol. 209. The central nervous system control of respiration; 2014. p. 379-406.

Holstege, G.; Kuypers, HGJM. The anatomy of brain stem pathways to the spinal cord in cat. A labeled amino acid tracing study. In: Kuypers, HGJM.; Martin, GF., editors. Progr Brain Res. Vol. 57. Elsevier; Amsterdam: 1982. p. 145-175.Descending pathways to the spinal cord

Holstege G, Kuypers HG, Boer RC. Anatomical evidence for direct brain stem projections to the somatic motoneuronal cell groups and autonomic preganglionic cell groups in cat spinal cord. Brain Res. 1979; 171:329–333. [PubMed: 466446]

Huma Z, Du Beau A, Brown C, Maxwell DJ. Origin and neurochemical properties of bulbospinal neurons projecting to the rat lumbar spinal cord via the medial longitudinal fasciculus and caudal ventrolateral medulla. Front Neural Circuits. 2014 doi: 10.3389/fncir.2014.00040.

Jones BE, Yang TZ. The efferent projections from the reticular formation and the locus coeruleus studied by anterograde and retrograde axonal transport in the rat. J Comp Neurol. 1985; 242:56–92. [PubMed: 2416786]

Kasumacic N, Lambert FM, Coulon P, Bras H, Vinay L, Perreault MC, Glover JC. Segmental organization of vestibulospinal inputs to spinal interneurons mediating crossed activation of thoracolumbar motoneurons in the neonatal mouse. J Neurosci. 2015; 35:8158–8169. [PubMed: 26019332]

Kiehn O. Locomotor circuits in the mammalian spinal cord. Annu Rev Neurosci. 2006; 29:279–306. [PubMed: 16776587]

Lakke EA. The projections to the spinal cord of the rat during development: a timetable of descent. Adv Anat Embryol Cell Biol. 1997; 135:1–143.

Lawrence DG, Kuypers HG. The functional organization of the motor system in the monkey. II. The effects of lesions of the descending brain-stem pathways. Brain. 1968; 91:15–36. [PubMed: 4966860]

Leong SK, Shieh JY, Wong WC. Localizing spinal-cordprojecting neurons in adult albino rats. J Comp Neurol. 1984a; 228:1–17. [PubMed: 6434598]

Leong SK, Shieh JY, Wong WC. Localizing spinal-cordprojecting neurons in neonatal and immature albino rats. J Comp Neurol. 1984b; 228:18–23. [PubMed: 6480907]

Liang H, Paxinos G, Watson C. Projections from the brain to the spinal cord in the mouse. Brain Struct Funct. 2011; 215:159–186. [PubMed: 20936329]

Liang H, Watson C, Paxinos G. Projections from the oral pontine reticular nucleus to the spinal cord of the mouse. Neurosci Lett. 2015; 584:113–118. [PubMed: 25459287]

Lingenhohl K, Friauf E. Giant neurons in the rat reticular formation: a sensorimotor interface in the elementary acoustic startle circuit? J Neurosci. 1994; 14:1176–1194. [PubMed: 8120618]

Martin GF, Humbertson AO Jr, Laxson LC, Panneton WM, Tschismadia I. Spinal projections from the mesencephalic and pontine reticular formation in the North American opossum: a study using axonal transport techniques. J Comp Neurol. 1979; 187:373–399. [PubMed: 489785]

Martin GF, Cabana T, Waltzer R. The origin of projections from the medullary reticular formation to the spinal cord, the diencephalon and the cerebellum at different stages of development in the North American opossum: studies using single and double labeling techniques. Neuroscience. 1988; 25:87–96. [PubMed: 3393288]

Masson RL, Sparkes ML, Ritz LA. Descending projections to the rat sacrocaudal spinal cord. J Comp Neurol. 1991; 302:120–130. [PubMed: 1856316]

Matsuyama K, Kobayashi Y, Takakusaki K, Mori S, Kimura H. Termination mode and branching patterns of reticuloreticular and reticulospinal fibers of the nucleus reticularis pontis oralis in the cat: an anterograde PHA-L tracing study. Neurosci Res. 1993; 17:9–21. [PubMed: 8414221]

Matsuyama K, Mori F, Kuze B, Mori S. Morphology of single pontine reticulospinal axons in the lumbar enlargement of the cat: a study using the anterograde Tracer PHA-L. J Comp Neurol. 1999; 410:413–430. [PubMed: 10404409]

Mitani A, Ito K, Mitani Y, McCarley RW. Descending projections from the gigantocellular tegmental field in the cat: cells of origin and their brainstem and spinal cord trajectories. J Comp Neurol. 1988; 268:546–566. [PubMed: 2451685]

Newman DB. Distinguishing rat brainstem reticulospinal nuclei by their neuronal morphology. II. Pontine and mesencephalic nuclei. J Hirnforsch. 1985; 26:385–418. [PubMed: 4067279]

Nudo RJ, Masterton RB. Descending pathways to the spinal cord: a comparative study of 22 mammals. J Comp Neurol. 1988; 277:53–79. [PubMed: 3198796]

Nyberg-Hansen N. Sites and mode of termination of reticulospinal fibers in the cat.An experimental study with silver impregnation methods. J Comp Neurol. 1965; 124:71–99. [PubMed: 14304275]

Oliva AA Jr, Jiang M, Lam T, Smith KL, Swann JW. Novel hippocampal interneuronal subtypes identified using transgenic mice that express green fluorescent protein in GABAergic interneurons. J Neurosci. 2000; 20:3354–3368. [PubMed: 10777798]

Pasqualetti M, Diaz C, Renaud JS, Rijli FM, Glover JC. Fate-mapping the mammalian hindbrain: segmental origins of vestibular projection neurons assessed using rhombomere-specific Hoxa2 enhancer elements in the mouse embryo. J Neurosci. 2007; 27:9670–9681. [PubMed: 17804628]

Paxinos, G.; Halliday, G.; Watson, C.; Koutcherov, Y.; Wang, H. Atlas of the developing mouse brain. 1st. Elsevier; Amsterdam: 2007.

Perreault MC, Glover JC. Glutamatergic reticulospinal neurons in the mouse: developmental origins, axon projections, and functional connectivity. Ann N Y Acad Sci. 2013; 1279:80–89. [PubMed: 23531005]

Petras JM. Cortical, tectal and tegmental fiber connections in the spinal cord of the cat. Brain Res. 1967; 6:275–324. [PubMed: 6060511]

Reiner K, Sukhotinsky I, Devor M. Bulbospinal neurons implicated in mesopontine-induced anesthesia are substantially collateralized. J Comp Neurol. 2008; 508:418–436. [PubMed: 18335539]

Rice CD, Weber SA, Waggoner AL, Jessell ME, Yates BJ. Mapping of neural pathways that influence diaphragm activity and project to the lumbar spinal cord in cats. Exp Brain Res. 2010; 203:205–211. [PubMed: 20186399]

Rye DB, Lee HJ, Saper CB, Wainer BH. Medullary and spinal efferents of the pedunculopontine tegmental nucleus and adjacent mesopontine tegmentum in the rat. J Comp Neurol. 1988; 269:315–341. [PubMed: 2453532]

Sakai ST, Davidson AG, Buford JA. Reticulospinal neurons in the pontomedullary reticular formation of the monkey (Macaca fascicularis). Neuroscience. 2009; 163:1158–1170. [PubMed: 19631726]

Satoh K. The origin of reticulospinal fibers in the rat: a HRP study. J Hirnforsch. 1979; 20:313–322. [PubMed: 536593]

Sengul G, Puchalski RB, Watson C. Cytoarchitecture of the spinal cord of the postnatal (P4) mouse. Anat Rec. 2012; 295:837–845.

Shen P, Arnold AP, Micevych PE. Supraspinal projections to the ventro-medial lumbar spinal cord in adult male rats. J Comp Neurol. 1990; 300:263–272. [PubMed: 2175317]

Sirkin DW, Feng AS. Autoradiographic study of descending pathways from the pontine reticular formation and the mesencephalic trigeminal nucleus in the rat. J Comp Neurol. 1987; 256:483–493. [PubMed: 3558885]

Sivertsen MS, Perreault MC, Glover JC. Characterization of rostral medullary and pontine reticulospinal projections in the late fetal and neonatal mouse. Soc Neurosci Abstr. 2013; 43:560.03.

Sivertsen MS, Glover JC, Perreault MC. Organization of pontine reticulospinal inputs to motoneurons controlling axial and limb muscles in the neonatal mouse. J Neurophysiol. 2014; 112:1628–1643. [PubMed: 24944221]

Stokke MF, Nissen UV, Glover JC, Kiehn O. Projection patterns of commissural interneurons in the lumbar spinal cord of the neonatal rat. J Comp Neurol. 2002; 446:349–359. [PubMed: 11954034]

Szokol K, Perreault MC. Imaging synaptically mediated responses produced by brainstem inputs onto identified spinal neurons in the neonatal mouse. J Neurosci Methods. 2009; 180:1–8. [PubMed: 19427523]

Szokol K, Glover JC, Perreault MC. Organization of functional synaptic connections between medullary reticulospinal neurons and lumbar descending commissural interneurons in the neonatal mouse. J Neurosci. 2011; 31:4731–4742. [PubMed: 21430172]

Tamamaki N, Yanagawa Y, Tomioka R, Miyazaki J-I, Obata K, Kaneko T. Development of mouse expressing GFP in GABAergic neurons. Neurosci Res. 2003; 25(Suppl):S77.

Tohyama M, Sakai K, Salvert D, Touret M, Jouvet M. Spinal projections from the lower brain stem in the cat as demonstrated by the horseradish peroxidase technique. I. Origins of the reticulospinal tracts and their funicular trajectories. Brain Res. 1979; 173:383–403. [PubMed: 487101]

Vanderhorst VG, Ulfhake B. The organization of the brainstem and spinal cord of the mouse: relationships between monoaminergic, cholinergic, and spinal projection systems. J Chem Neuroanat. 2006; 31:2–36. [PubMed: 16183250]

Watkins LR, Griffin G, Leichnetz GR, Mayer DJ. The somatotopic organisation of the nucleus raphe magnus and surrounding brain stem structures as revealed by HRP slow-release gels. Brain Res. 1980; 181:1–15. [PubMed: 7350948]

West MJ. New stereological methods for counting neurons. Neurobiol Aging. 1993; 14:275–285. [PubMed: 8367009]

Williams RW, Rakic P. Three-dimensional counting: an accurate and direct method to estimate numbers of cells in sectioned material. J Comp Neurol. 1988; 278:344–352. [PubMed: 3216047]

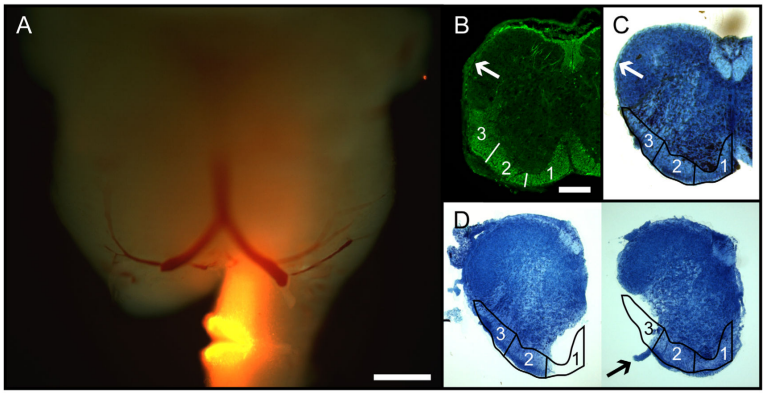

Figure 1.

Overview of retrograde labeling targeted to specific white matter zones. **A**: Whole-mount image of a P0 brainstem retrogradely labeled unilaterally at the level of the C2 ventral root, indicating how labeling was restricted to zone 1 and how contralateral contamination was stringently avoided by removing the uppermost part of the contralateral spinal cord. Diffuse fluorescence produced by retrogradely labeled neurons and axons can be discerned in both medulla and pons, most noticeably in the medial half of the ipsilateral medulla. The preparation is illuminated by both epifluorescence and incident white light to reveal tissue contours. **B**: Neurofilament immunostaining in a transverse section from the upper cervical spinal cord at P0, illustrating the distribution of axons in the white matter. Arrow indicates the dorsolateral fasciculus, which extends as a thin rind of white matter from the dorsal tip of the LF nearly to the dorsal midline (Sengul et al., 2012). Numbers 1–3 indicate the different zones used for selective retrograde labeling. **C**: Transverse section from the upper cervical spinal cord at P0, stained with methylene blue to show the white matter (light blue regions), with zones 1–3 (outlined) and the dorsolateral fasciculus (arrow) indicated. **D**: Transverse sections at C2 in preparations with labeling restricted to zone 1 (left) and zone 3 (right). Arrow in right panel indicates the C2 ventral root. Scale bars = 500 μm in A; 200 μm in B (applies to B–D).

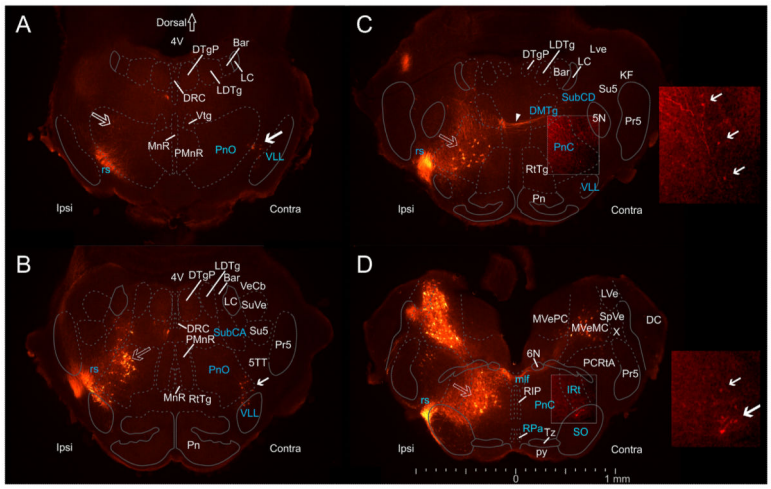

Figure 2.

Spatial distribution of pRS neurons and other neuron populations in the pons. Epifluorescence images (50-μm transverse sections, evenly spaced at 250-μm intervals through the pons at P0) showing retrograde labeling in the pons after applying RDA unilaterally (Ipsi) to the entire VF + LF at C2. Cytoarchitectonically defined boundaries of relevant nuclei and structures adapted from the atlas of Paxinos et al. (2007) have been superimposed (see Materials and Methods). Dashed lines indicate boundaries transferred from the Paxinos et al. (2007) atlas, which should thus be considered only as approximate, whereas solid lines indicate boundaries that could be seen in neighboring sections stained with methylene blue. **A**: Rostralmost section, showing ipsilateral pRS neurons in the PnO (open arrow) lying dorsal to the labeled axons of the rubrospinal tract (rs). Contralateral pRS neurons (solid arrow) lie near the lateral edge of the PnO, in the border area between the PnO and the ventral nucleus of the lateral lemniscus (VLL). **B**: At this level (250 μm more caudal than A), ipsilateral pRS neurons form a distinct cluster in the lateral half of the PnO, adjoining the more dorsal group of retrogradely labeled neurons in the nucleus subcoeruleus alpha part (SubCA). Contralateral pRS neurons lie in the ventrolateral corner of the PnO, similar to their location in A. **C**: Ipsilateral pRS neurons are located centrally in the PnC. A few contralateral pRS neurons are also labeled in the lateral part of the PnC. However, they are weakly labeled and are best seen in the **inset** displaying the same region at twice the magnification and with enhanced brightness and contrast (solid arrows indicate individual neurons). At this level, axons from contralateral pRS are seen traversing the PnC, the SubCD, and the dorsomedial tegmental area (DMTg) before crossing the midline (arrowhead). **D**: In the most caudal region of pons, ipsilateral pRS neurons lie centrally within the PnC where they are enmeshed with labeled axons coursing toward the spinal cord. Contralateral pRS neurons are located near the ventrolateral corner of the PnC, in a region that according to Paxinos et al. (2007) corresponds to the superior olive (SO) and the intermediate reticular nucleus (IRt). They are also shown in the **inset** at right. At this level, ipsilateral and contralateral vestibulospinal neurons can also be seen clearly. Note that the location of contralateral pRS neurons outside the indicated confines of the PnO is in our view due to a combination of shifts in the locations of boundaries from the illustrated section

to the adjacent methylene blue-stained section and ambiguity in the transfer of the boundaries defined by Paxinos et al. (2007).

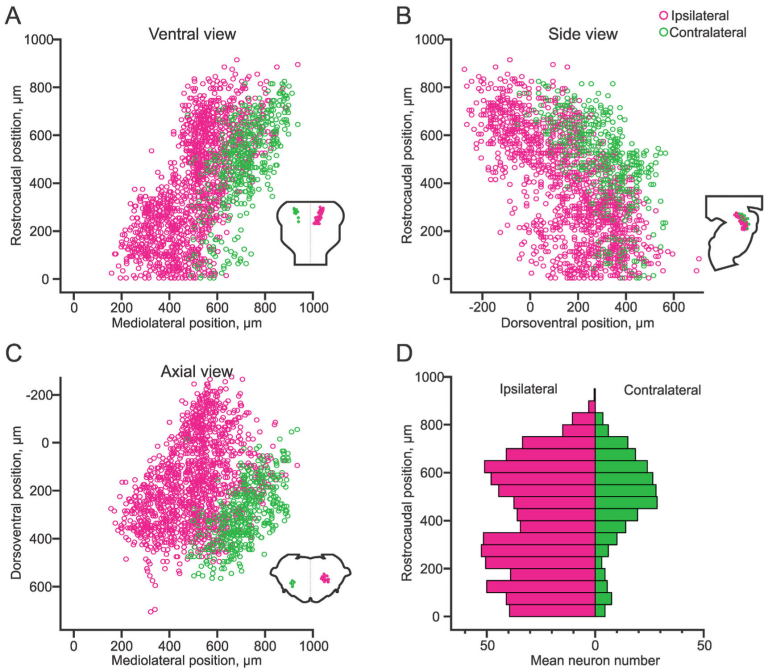

Figure 3.

Spatial relationship between the ipsilateral and contralateral pRS neuron populations. A–C: Plots showing the positions of individual pRS neurons pooled from two preparations in different planes of view (**insets**). Magenta and green circles indicate ipsilateral and contralateral pRS neurons, respectively. Note that both pRS neuron populations are plotted on the same side to emphasize the difference in spatial domains. Because the plots are obtained from parasagitally sectioned preparations, for which mediolateral coordinates automatically become discontinuous according to the spacing of the sections, the mediolateral coordinates have been randomized through the section thickness to provide a smoother representation. **A**: Plot of rostrocaudal vs. mediolateral position of each labeled pRS neuron (ventral view). The origin is placed at the point where the midline and the medulla/pons transition meet. **B**: Plot of rostrocaudal vs. dorsoventral position of each labeled pRS neuron (side view). The origin is placed at the point where the ventralmost extent of the fourth ventricle and the medulla/pons transition meet. **C**: Plot of dorsoventral vs. mediolateral position of each labeled pRS neuron (axial view). The origin is placed at the point where the ventralmost extent of the fourth ventricle and the midline meet. **D**: Histogram of the number of pRS neurons along the rostrocaudal extent of the pons (divided into 50-µm bins). The value in each bin represents the mean number of neurons in the two preparations.

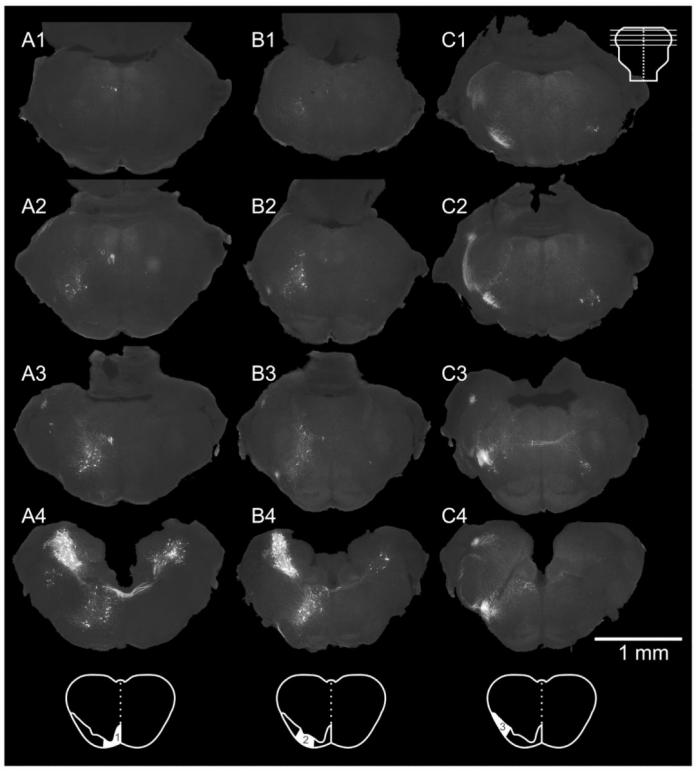

Figure 4.

Spatial distribution of pRS neurons that project in different white matter zones. Columns A–C show the spatial distribution of pRS neurons in preparations retrogradely labeled from zone 1 (A1–4), zone 2 (B1–4), and zone 3 (C1–4), respectively. Each column includes four transverse sections evenly spaced at 250-μm intervals through the pons, at the levels indicated in the **inset** at top. **A1–4**: Zone 1 labels preferentially the ipsilateral pRS neuron population, relatively more at caudal than at rostral levels. **B1–4**: Zone 2 labels both the ipsi- and contralateral pRS populations, in a pattern similar to that seen in preparations labeled from the VF + LF (see Fig. 2). **C1–4**: Zone 3 labels preferentially the contralateral pRS neuron population but also some rostral ipsilateral pRS neurons. Note the axons of the contralateral pRS neurons crossing the midline in C3. Scale bar = 1 mm.

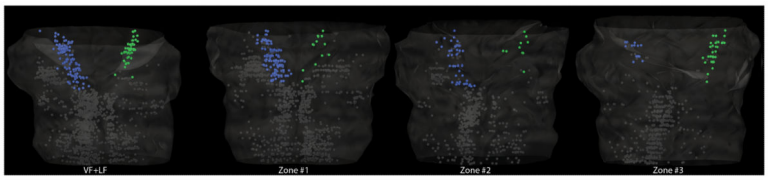

Figure 5.

3D reconstructions of pRS neurons labeled differentially from different white matter zones. Four 3D reconstructions, one for each tracer application employed (VF + LF, zones 1–3), generated with the Neurolucida Solids modeling module. Ipsilateral pRS neurons are blue, contralateral pRS neurons are green, and other neurons (including vestibulospinal and medullary reticulospinal) are gray. The surface of each reconstruction (transparent white) has been generated from section outlines. In the VF + LF reconstruction, contralateral pRS neurons are concentrated in the caudal portion of the pons, whereas the ipsilateral pRS population is larger and more evenly distributed along the rostrocaudal axis. In the zone 1–3 reconstructions, ipsilateral pRS neurons are mainly labeled from zones 1 and 2, whereas contralateral pRS neurons are mainly labeled from zone 3.

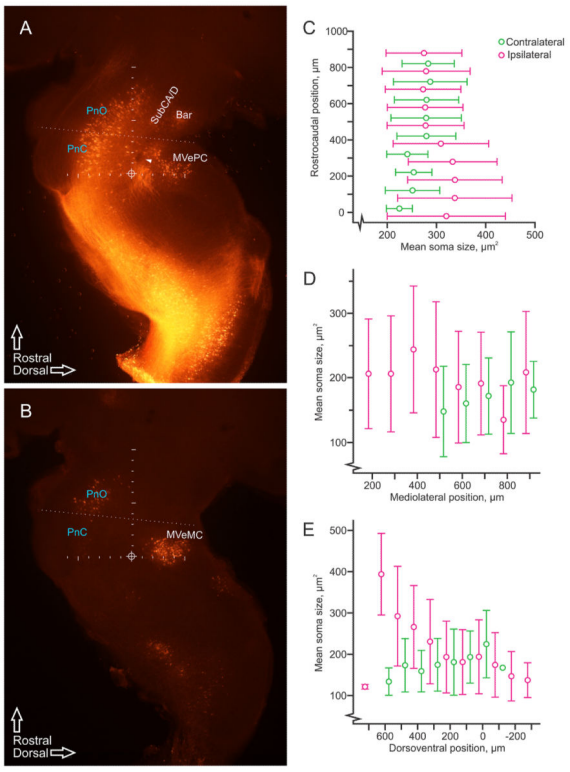

Figure 6.

Regional variation of pRS neuron soma size. **A**: Image of retrogradely labeled ipsilateral neurons and axons, including the ipsilateral pRS neurons and axons, from four adjacent parasagittal 50-µm sections (taken between 400 and 600 µm from the midline) projected onto a single layer. The ipsilateral pRS population can be seen as a continuous band of labeled neurons that starts around the pons/medulla transition (horizontal line of tick marks, 100-µm intervals) and that follows the natural curvature of the pons rostrally. It thus extends from the PnC to the PnO, which we have operationally defined as, respectively, caudal and rostral to the oblique dotted line. Clusters of neurons that were not considered part of the pRS are also labeled, including those in the nucleus subcoeruleus alpha and dorsal parts (SubCA/D), Barrington's nucleus (Bar), and medial vestibulospinal nucleus, parvocellular part (MVePC). The genu of the facial nerve can be seen as a dark spot (arrowhead) to the left of the vertical line of tick marks (100-µm intervals) that has been used as the rostrocaudal axis in all figures. The circled cross indicates the intersection of the vertical and the dorsoventral axes and represents the origin of both, as used in the graphs presented in other figures. **B**: Image of retrogradely labeled contralateral neurons and axons, including the contralateral pRS neurons and axons, from adjacent parasagittal 50-µm sections (taken from 600 to 800 µm from the midline) projected onto a single layer. Axes and division between PnC and PnO as in A. Also labeled are neurons in the medial vestibulospinal nucleus, magnocellular part (MVeMC). **C–E**: Graphs displaying soma sizes of pRS neurons (magenta: ipsilateral, green: contralateral) measured in the parasagittal plane in 100-µm bins along the rostrocaudal axis (C), mediolateral axis (D), and dorsoventral axis (E). Circles indicate mean values, and error bars represent standard deviations.

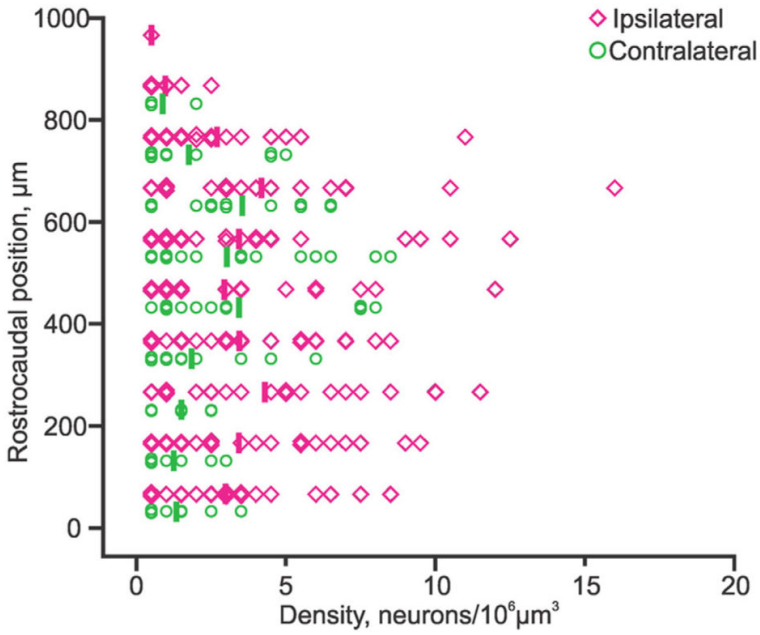

Figure 7.

pRS neuron density along the rostrocaudal axis. Graph showing density of ipsilateral (magenta lozenges) and contralateral (green circles) pRS neurons measured in 100-µm-on-a-side cubes along the rostrocaudal axis. Densities averaged below 5 neurons/10^6 µm^3 but could reach over 10 neurons/10^6 µm^3. For example, the single highest density (the magenta lozenge within the 600–700-µm bin) matches well the densely populated area indicated by the open arrow in Figure 2B.

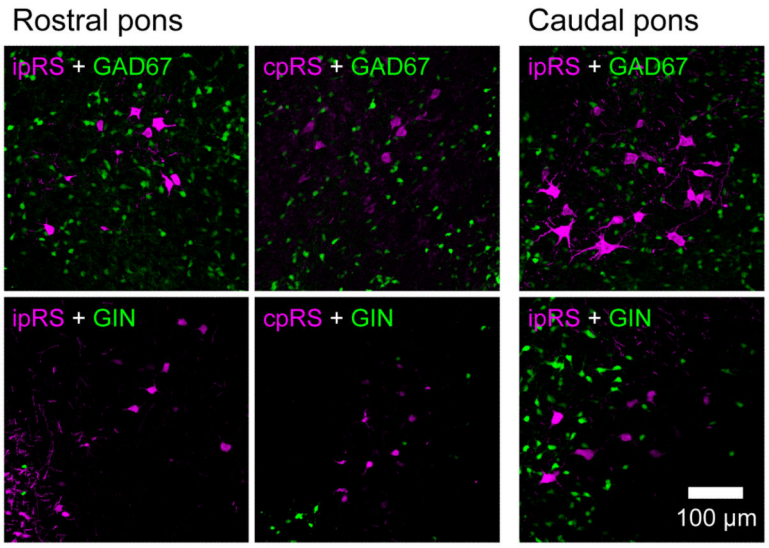

Figure 8.

Distribution of putative GABAergic neurons among the pRS neurons. Collapsed confocal image stacks of 14-µm transverse sections from the rostral PRF (four left images) and caudal PRF (two right images). Retrograde labeling was performed in GAD67 (top row) and GIN (bottom row) GFP reporter mice. Green, GAD67- or GIN-expressing cells. Magenta, ipsilateral or contralateral pRS neurons (ipRS, cpRS). Note that GFP^{+} neurons within the PRF are much more numerous in GAD67 than in GIN reporter mice, a presumed consequence of the differences in the subtypes of putative GABAergic neurons that express GFP in these two transgenic mouse strains. In neither strain did we find pRS neurons that were positive for GFP. Scale bar = 100 mm.

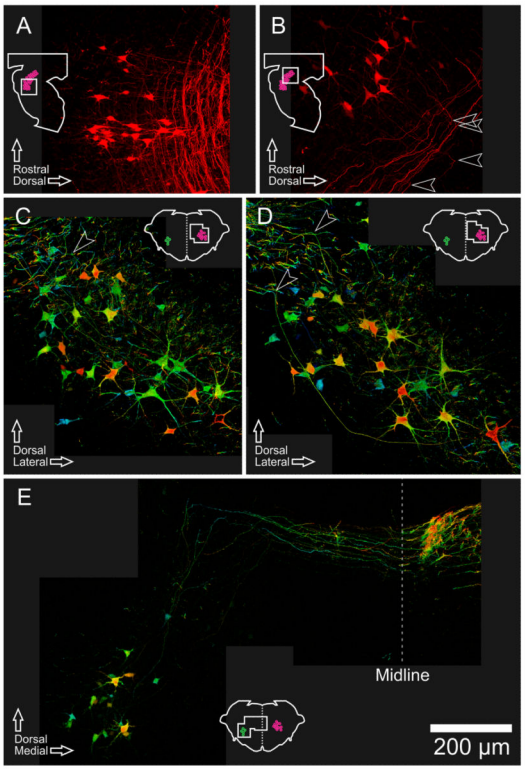

Figure 9.

pRS axon trajectories within the brainstem. Collapsed confocal image stacks of 50-µm sections, showing pRS neurons and their axon trajectories. **Insets** show planes and regions of view. **A:** Oblique longitudinal section cut at an angle of approximately 35 ° to the parasagittal plane, showing caudal ipsilateral pRS neurons and their axons. **B**: Parasagittal section showing rostral ipsilateral pRS neurons and their axons. Arrowheads indicate the sharp 90 ° turns made by the axons as they begin their descent toward the spinal cord. **C,D**: Transverse sections showing ipsilateral pRS neurons and their axons, with color coding for rostrocaudal depth within the section (blue is rostral, red is caudal). Examples can be seen of pRS axons that traverse much of the image within the same plane (constant color) before turning abruptly (changing color rapidly, arrowheads) and leaving the section. **E**: Oblique transverse section through the rostral pons (oriented radially from ventricular to pial surface according to the curvature of the pons) showing contralateral pRS neurons and their axons. Several individual axons can be followed for different distances dorsally and then medially within the same transverse plane (constant color) before crossing the midline and beginning their descent toward the spinal cord. Scale bar = 200 µm.

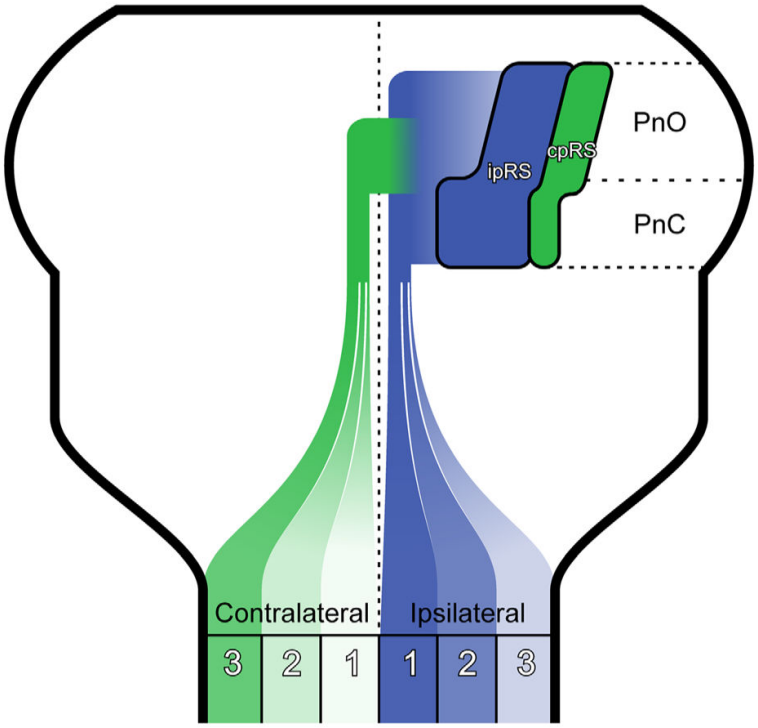

Figure 10.

Summary figure. Cartoon illustrating some of the major findings in this study. Ipsilateral and contralateral pRS neuron populations (blue, ipRS; green, cpRS) are drawn as shapes that roughly represent their relative positions and neuron numbers. IpRS neurons are numerous at all rostrocaudal levels, whereas cpRS neurons are more numerous in the rostral than in the caudal pons. The relative distributions of ipRS and cpRS axons in the three zones of the white matter are indicated by color saturation, with the darkest and lightest colors indicating highest and lowest number of axons, respectively.

TABLE 1

Antibodies Used in This Study

Antibody name	Type	Host species	Dilution	Company	Catalog No.	RRID	Specificity
Tetramethylrhodamine	Polyclonal	Rabbit	1:1,000	Invitrogen	A-6397	AB_1502299	Quenches > 50% of tetramethylrhodamine fluorescence, cross-reactivity with Texas red and rhodamine red dyes
Pan-neuronal neurofilament	Monoclonal	Mouse	1:5,000	Covance	SMI-311R-100	AB_10143907	Nonphosphoneurofilaments, mammalian
Alexa 555 goat anti-rabbit	Polyclonal	Goat	1:400	Invitrogen	A21428	AB_141784	Rabbit IgG, H + L chains

TABLE 2

Estimated Numbers (Mean ± SD) of Labeled Ipsilateral and Contralateral pRS Neurons Counts

Estimates from size analysis and direct counts			Estimates from 3D reconstructions and direct counts							
	VF + LF (n = 5)			VF + LF (n = 3)		Zone 1 (n = 4)		Zone 2 (n = 3)		Zone 3 (n = 3)	
Laterality	**Ipsilateral**	**Contralateral**		**Ipsilateral**	**Contralateral**	**Ipsilateral**	**Contralateral**	**Ipsilateral**	**Contralateral**	**Ipsilateral**	**Contralateral**
Above line	331 ± 90	153 ± 29[1]	PnO	376 ± 65	184 ±70[3]	234 ± 31[5]	28 ± 19[5]	153 ± 19	67 ± 16[3]	48 ± 45	174 ± 27[3]
Below line	320 ± 72	48 ± 16 [1,2]	PnC	352 ± 70	28 ± 23[3, 4]	332 ± 172[5]	9 ± 14	132 ± 21	21 ± 13[3]	13 ± 14	68 ± 58[4]
Sum	651± 152	200 ±42[1]		728 ±49	212±56[3]	567 ± 185[5]	37 ± 30[5]	285 ± 3	88 ± 27[3]	61 ± 32	242 ± 40[3]

[1] $P < 0.001$ contralateral different from ipsilateral, Mann-Whitney U test (n = m = 5, U = 0).

[2] $P < 0.01$ above line different from below line, Mann-Whitney U test (n = m = 5, U = 0).

[3] $P < 0.01$ contra different from ipsi, Mann-Whitney U test (n=m = 3, U = 0).

[4] $P < 0.01$ PnO different from PnC, Mann-Whitney U test (n = m = 3, U = 0).

[5] $P < 0.01$ zone 1 different from zone 3, Mann-Whitney U test (n = 4, m = 3, U = 0).